Journal of Molecular Catalysis A: Chemical 300 (2009) 41–47

Contents lists available at ScienceDirect

Journal of Molecular Catalysis A: Chemical

journal homepage: www.elsevier.com/locate/molcata

The formation mechanism of Mo-methylidene species over Mo/HBeta catalysts for heterogeneous olefin metathesis: A density functional theory study

Jing Guan[a], Gang Yang[a], Danhong Zhou[a,b], Weiping Zhang[a], Xianchun Liu[a], Xiuwen Han[a], Xinhe Bao[a,*]

[a] State Key Laboratory of Catalysis, Dalian Institute of Chemical Physics, Chinese Academy of Sciences, Dalian 116023, People's Republic China
[b] Institute of Chemistry for Functionalized Materials, College of Chemistry and Chemical Engineering, Liaoning Normal University, Dalian 116029, People's Republic China

ARTICLE INFO

Article history:
Received 5 May 2008
Received in revised form 10 October 2008
Accepted 15 October 2008
Available online 7 November 2008

Keywords:
Active sites
Density functional calculations
Mo/HBeta catalysts
Olefin metathesis
Oxidation states

ABSTRACT

Density Functional Theory (DFT) calculations were performed to optimize the Mo active sites in HBeta zeolite catalysts as well as to locate the reaction pathways to form the Mo-methylidene species. Two different Mo active sites, i.e., the oxidized $Mo^{VI}O_2$ and its reduced form $Mo^{V}O(OH)$, were developed and incorporated into HBeta zeolites by replacing a pair of Brønsted acidic sites. The Mo-methylidene species were found to be produced through two elementary reaction steps, and the Mo-oxametallacyclobutanes were identified as the intermediates. The activation barriers of the decompositions of the oxametallacyclobutane intermediates (Step 2) were estimated to be higher than those of the ethene addition on the Mo active sites (Step 1). The oxidation states of the Mo centers exerted marked influences on the stabilities of the intermediates as well as on the activation barriers and reaction heats of Steps 1 and 2, which were elucidated by the electronic properties of the O_b-ligands directly bonded to the Mo centers. Both free energy barriers and reaction heats have indicated that the whole processes of generating the Mo-methylidene species were preferred over the Mo(VI) rather than Mo(V) active site. Accordingly, the Mo(VI) active site was more efficient in catalyzing the formation of Mo-methylidene species in the heterogeneous Mo/HBeta catalytic systems.

1. Introduction

Zeolites are three-dimensional aluminosilicates with molecular-dimension cages and channels acting as micro-reactors. The loading of molybdenum (Mo) species into the acidic sites of zeolites enhances their performances in many catalytic processes, such as selective oxidation, hydrodesulfurization and metathesis [1–5]. Recently, our laboratory has reported that the Mo-loaded HBeta zeolite exhibits activities for the metathesis reaction of ethene and 2-butene to form propene [6,7]. Addition of alumina into the HBeta zeolite resulted in a proportion of the Mo species preferentially migrating into the alumina phase. A higher reactivity was thus obtained compared to the pure zeolite catalysts [7].

The metal-carbene species are usually acknowledged as the initiating and propagating intermediates in olefin metathesis, as described by the Hérisson-Chauvin mechanism [8–10]. However, it is still unclear how the metal-carbene species is formed on the metal-supported catalysts [8,9,11–19]. The dynamic counting experiments indicated that in the highly dispersed Mo/Al_2O_3 catalysts, less than 1% Mo sites are active for the propene metathesis [20,21]. It thus becomes challenging to detect the Mo active sites with the current spectroscopy techniques. Very recently, Salameh et al. [22] have studied the reaction of Re_2O_7/Al_2O_3 catalysts with various olefins and shown that the creation of Re-carbene species does not require an allylic olefin. A four-membered oxametallacyclobutane structure was considered to act as the intermediate, which was formed and then decomposed to produce metal-carbene species. A large number of quantum chemical calculations have been devoted to the mechanistic studies on ethene addition to OsO_4 and ReO_3L (L denotes the ligand) to produce the metallaoxetane intermediates [19,23–28]. As to the Mo-based catalysts, only few computational studies were conducted on the homogeneous systems. Rappé and Goddard [11,29] investigated the activation process of ethene by the simple $Mo^{VI}O_2Cl_2$ complex via the pseudo-Wittig mechanism. What will happen if the complex is switched to the heterogeneous Mo-based HBeta zeolite catalysts? It is a question worthy of further investigations. Furthermore, most of the previous theoretical calculations focused on the metallaoxetane intermediates, while the important process of dissociating the metallaoxetane intermediates to form the metal-carbene species has not received enough attention.

* Corresponding author. Tel.: +86 411 84686637; fax: +86 411 84694447.
E-mail address: xhbao@dicp.ac.cn (X. Bao).

1381-1169/$ – see front matter © 2008 Elsevier B.V. All rights reserved.
doi:10.1016/j.molcata.2008.10.044

In this work, the whole reaction processes from the Mo active sites to the Mo-carbene species were investigated with the aid of density functional calculations. The Mo/HBeta zeolite was used as the catalyst. The activation barriers of the two reaction steps, i.e., the formations of the metallaoxetane intermediates from the Mo active sites as well as the Mo-carbene species from the decomposition of the metallaoxetane intermediates, were obtained. Owing to their low concentrations as described above, the oxidation states of the Mo active sites still remain pendent. Grüenert et al. [30,31] considered that the Mo(VI) active sites were responsible for the reactivity whereas the Mo(V) species were the by-products. On the contrary, the ESR results obtained by Jin's group [32] supported the Mo(V) active sites. The Mo(IV) species were also claimed to be active sites in the Mo/SiO_2 catalysts prepared via the fixation of organometallic complexes [12,33,34] or by photo-reduction [8,9,35,36]. In our *in situ* ESR studies (in preparation), the intensity of the Mo(V) peak became stronger upon exposure to alkene atmosphere under reaction conditions, which was caused by the reduction of Mo(VI) sites. The *in situ* XPS studies of ours further pointed out that the Mo(IV) signals were detected after a long reaction period, accompanied by the deactivation of the catalysts. Accordingly, the Mo(IV) species may be the precursors but unlikely to be active sites. The possible Mo(V) and Mo(VI) active sites were considered here to initiate the metathesis reactions, which were incorporated into HBeta zeolite by replacing a pair of Brønsted acidic sites. Parallel density functional calculations of the two oxidation states were performed on the whole reaction pathways. On the basis of these calculations, the electronic properties of the oxygen ligands bonded to the Mo(V) and Mo(VI) sites were studied, providing insights into the relative stabilities of the oxametallacyclobutane intermediates as well as the energy barriers of the elementary reaction steps.

2. Computational details

2.1. Cluster models

The Beta zeolite models were taken from the framework structure of polymorph A reported by Newsam et al. [37]. Beta zeolite has two straight channels (0.76 nm × 0.64 nm) perpendicular to each other and another helical channel (0.55 nm × 0.55 nm) perpendicular to the previous two. The three channels intersect with each other and form the open pore systems [38]. The β-site (Fig. 1) consisting of planar deformed six-membered rings (6-MR) represents the most stable and preferable location of transition metal ions in HBeta zeolite. The visible and FTIR spectral studies on the Co(II) sited in dehydrated HBeta zeolite suggested that the Co^{II} ions predominated in the β-sites where two framework Al atoms were situated nearby [39]. In addition, the recent quantum chemical calculations of Zn(II)-exchanged HBeta zeolite indicated that a majority of Zn(II) ions were located at the six-membered rings, and the results were confirmed by the EXAFS experiments [40]. Thus the β-sites in HBeta zeolite were chosen here to hold the exchanged Mo ions. The ^{27}Al MQ MAS NMR results showed that Al atoms in T1 and T2 sites of HBeta zeolite resisted dealumination and accordingly did not adopt octahedral oxygen coordination, suggesting that these two sites were energetically favoured over the other T sites [41]. As shown in Fig. 1, the geometries of the T1 and T2 sites in the six-membered rings are quite similar, and the two T1 sites were replaced by the Al atoms. The two T1 sites are next-next-nearest neighbors (NNNN) to each other, which obey the Lowenstein's rule.

The cluster approaches have been proven sufficient to reproduce the properties and catalysis of metal-exchanged zeolites [42–46]. In this work, the Mo-exchanged Beta zeolites were represented by clusters containing 10 T sites, which were much larger than the commonly used 5 T clusters [42,46]. Similar Beta cluster models were used by Pietrzyk et al. [47] to study the properties and reactivities of the V^VO_2-exchanged Beta zeolite. The clusters were terminated by H atoms bonded to O or Si atoms, directing towards what would have been the next zeolite framework atoms. The terminal Si–H and O–H distances were fixed at 1.500 and 1.000 Å, respectively. The terminal H, O and Si atoms were kept fixed during the geometry optimizations in order to retain the local geometries of Beta zeolite, while the other atoms were allowed to relax fully so as to consider the deformations of the zeolite frameworks induced by the extra-framework species.

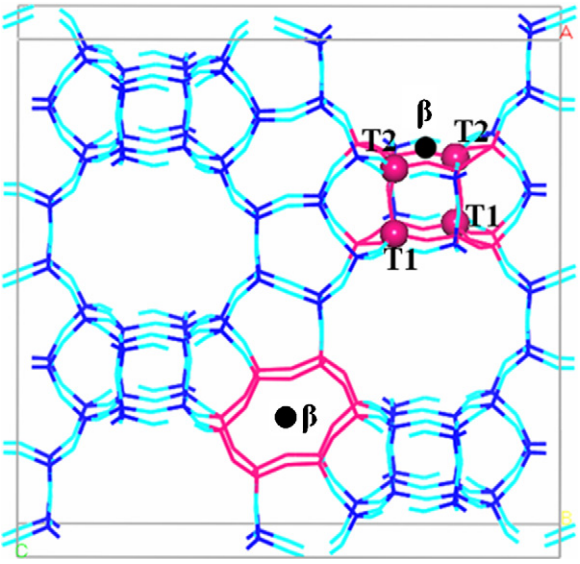

Fig. 1. The locations of β-sites consisting of planar deformed six-membered rings (6-MR) in Beta zeolite.

2.2. Theoretical methods

Density functional theory calculations were performed using the nonlocal three-parameter B3LYP density functional, which combines the Becke's exchange [48,49] and Lee, Yang and Parr's correlation functionals [50,51]. The LANL2DZ basis set with relativistic effective core potential (RECP) of Hay and Wadt [52] was used to describe the Mo element, and the 6-31G(d,p) basis set for all the remaining elements. Such a combination was designated as basis set 1 (B1). The structures were optimized without any symmetry constraints, and frequency calculations at the same level of theory (B3LYP/B1) were carried out to ensure that all the stationary points (reactant, products and intermediates) possess no imaginary vibrations and the transition states each possess only one imaginary vibration. The Gibbs free energies corrected by zero point energies (ZPE) were computed from the harmonic frequencies at 400 K and 1 atm, consistent with the experimental conditions [6]. The atomic charges were obtained using the Mulliken Population Analysis (MPA) scheme.

The above computational methods (B3LYP/B1) have been reported to obtain satisfactory results for late-transition-metal reactions [53]. To further confirm the reliability of B3LYP/B1 methods, some important structures were also optimized with larger basis set (B2). The details of the B2 basis set were as follows: The same RECP as in B1 was used for Mo, augmented with a f-polarization function (exponent 1.043) [54], and the other atoms were described by the 6-31 + G(d,p) basis set. As elucidated in the forthcoming Section 3, the B3LYP/B2 geometries showed quite similar features to those of the B3LYP/B1 methods. The total and relative

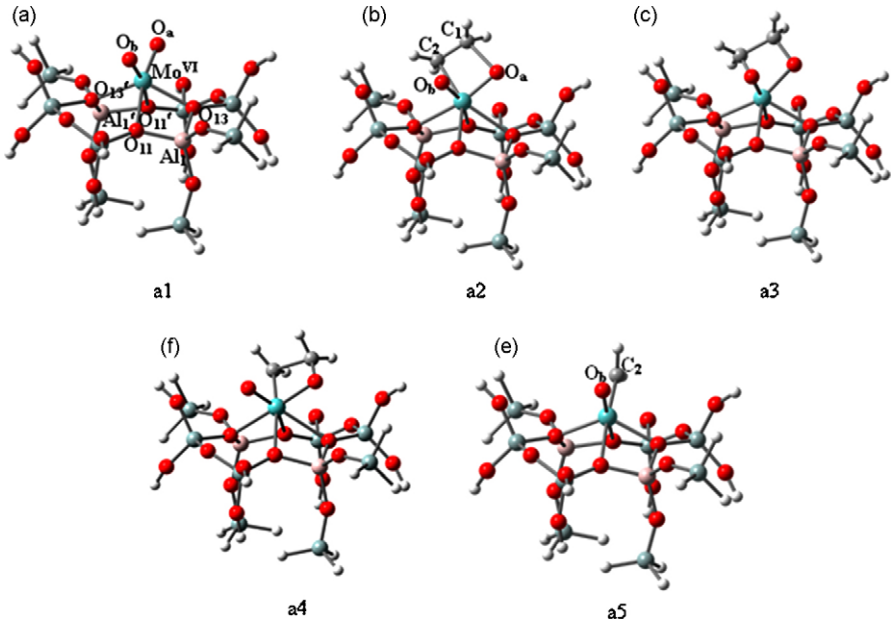

Fig. 2. The minima (**a1**, **a3**, **a5**) and the transition states (**a2**, **a4**) along the Mo(VI)-methylidene formation pathway.

energies were computed at the B3LYP/B2//B3LYP/B1 level of theory, since the recent calculations [23,55] of metal-oxide additions to olefins have shown that the B3LYP/B2 energies were in excellent agreements with the CCSD(T) theoretical and the experimental results.

All the calculations were performed with the Gaussian98 software package [56].

3. Results and discussion

3.1. Geometric structure of the Mo(VI) active site

The Mo/HBeta catalysts were prepared by impregnation of HBeta with aqueous ammonium heptamolybdate (AHM) solution. By calcinating the sample at high temperature, $MoO_2(OH)_2$ precursors, which may result from the decomposition of AHM, can migrate into the zeolite channels, where it reacts with the acidic proton to form the $MoO_2(OH)^+$ active sites. At even higher temperatures, the $MoO_2(OH)^+$ active sites can further react with a vicinal Brønsted acidic proton to form the $MoO_2{}^{2+}$ active sites within zeolite pores, as shown in the reaction below [57–59].

$$H^+Z^-Z^-H^+ + H_2M_OO_4 \rightarrow Z^-M_OO_2{}^{2+}Z^- + 2H_2O$$

The energy-minimum and transition-state structures along the reaction path of ethene addition to the Mo(VI) active site **a1** to form the Mo-methylidene species **a5** are presented in Fig. 2, with the important geometrical parameters listed in Table 1. The Mo(VI) active site possesses a symmetrical dioxo structure anchored by the lattice-O atoms. The distances between the Mo and dioxo O atoms (O_a and O_b) are about 1.70 Å, characteristic of Mo=O double bonds. As deduced from the Mo–O_z distances (O_z from the zeolite lattices), the Mo(VI) center forms four direct bonds with the O_z atoms belonging to the six-membered ring, consistent with the recent quantum mechanics results on various transition-metal-ion (TMI)-zeolite systems [60–64]. Moreover, the minimal Mo—O_z bond length is found equal to 2.122 Å and the Mo–Al distances are equal to 3.078 Å, which are also in agreement with the previous results of the Mo species encaged in other zeolites [65,66].

3.2. Mo-methylidene formation over the Mo(VI) active site

According to the pseudo-Wittig mechanism shown in Scheme 1a, the first stage is the formation of the oxamolybdacyclobutane intermediate **a3**. As the optimized geometries indicated, **a3** exhibits a trigonal bipyramidal (TBP) geometry. The oxo-O_b and lattice-O_{11}' atoms are the apical ligands. The three equatorial-O and Mo atoms fall almost within the same plane, which can be observed from the summed $\angle O_{11}$–Mo–O_a, $\angle O_a$–Mo–C_2 and $\angle C_2$–Mo–O_{11} angles with the value of 359.1°. The oxamolybdacyclobutane intermediate **a3** results from the [2 + 2] cycloaddition of Mo=O_a in the Mo(VI) active site **a1** and C_1=C_2 in ethene. New Mo—C_2 and C_1—O_a bonds are formed with the distances optimized at 2.229 and 1.429 Å, respectively. Meanwhile,

Table 1
Geometric parameters and Mulliken charges for the energy minima and transition states along the Mo(VI)-methylidene formation pathway[a].

	a1	a2	a3[b]	a4	a5
Mo–O_b	1.695	1.692	1.688 (1.677)	1.674	1.677
Mo–O_{11}	2.348	2.239	2.301 (2.300)	2.299	2.340
Mo–O_{11}′	2.348	2.489	2.385 (2.390)	2.560	2.333
Mo–O_{13}	2.122	2.383	2.185 (2.186)	2.434	2.146
Mo–O_{13}′	2.122	2.274	2.178 (2.169)	2.250	2.165
Mo–O_a	1.695	1.783	1.936 (1.917)	2.030	
C_1–C_2		1.422	1.513 (1.514)	2.028	
Mo–C_2		2.321	2.229 (2.221)	1.985	1.934
O_a–C_1		1.890	1.429 (1.432)	1.330	
O_b–Mo–O_{11}′	166.7	155.5	166.9 (167.4)	144.6	166.2
Mo–C_2–O_a–C_1		−164.3	−164.5 (−167.8)	178.4	
$\Sigma\alpha$[c]		359.3	359.1 (359.3)	359.8	
q(Mo)	1.52	1.25	1.33	1.32	1.25
q(O_a)	−0.42	−0.53	−0.58	−0.48	
q(O_b)	−0.42	−0.42	−0.42	−0.38	−0.41
q(MoO_2)	0.69	0.30	0.34	0.46	
q(C_1)	−0.43	−0.028	0.13	0.00	
q(C_2)	−0.43	−0.39	−0.43	−0.50	−0.43
q(C_2H_4)	0.00[d]	0.40	0.32	0.29	

[a] Bond distances in Å and angles, dihedrals in degrees.
[b] The data in parentheses are from the B3LYP/B2 methods.
[c] The sum of the three angles O_{11}–Mo–O_a, O_a–Mo–C_2 and C_2–Mo–O_{11}.
[d] The data for the isolated ethene molecule.

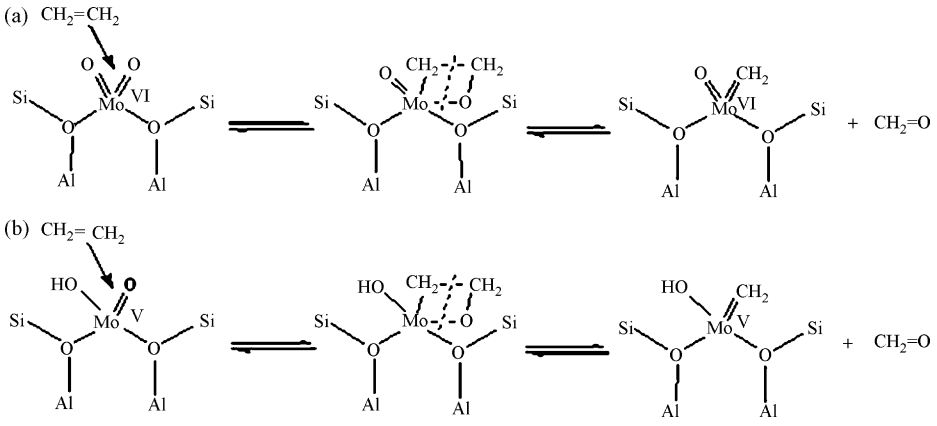

Scheme 1. Proposed pseudo-Wittig mechanism to produce the Mo-methylidene species with the Mo precursors as (a) $Mo^{VI}O_2$ and (b) $Mo^{V}O(OH)$, respectively.

the original Mo=O_a and C_1=C_2 double bonds are severely impaired and turn to single bonds (see the exact values in Table 1). That is, four single bonds constitute the $MoO_aC_1C_2$ oxamolybdacyclobutane ring in the intermediate **a3**. As the data in Table 1 showed, the geometric parameters at B3LYP/B1 and B3LYP/B2 levels are quite close to each other, and therefore the additional polarization functions exert slight influences on the geometries. The **a1** and **a3** stationary points are connected with the transition state **a2**, which has more features alike to **a3** rather than **a1**. In **a2**, the C_1—C_2 bond is elongated to 1.422 Å (vs. 1.330 Å in the isolated ethene molecule and 1.513 Å in **a3**), suggesting that the ethene molecule has been much activated. The oxo-O_b and lattice-O_{11}' ligands in **a2** are greatly tilted with the ∠O_b–Mo–O_{11}' angle calculated at 155.5°, different from the axial direction in **a3** (∠O_b–Mo–O_{11}' = 166.9°). It is caused by the long distance between the ethene fragment and Mo—O_a bond. A significant portion of the Mo—C_2 bond is formed in **a2** with the distance equal to 2.321 Å. It proves only 0.092 Å elongated compared with the corresponding bond in **a3**. However, the C_1—O_a distance is optimized at 1.890 Å, being 0.461 Å longer than that in **a3**. It indicates that the formation of the C_1—O_a bond lags far behind the Mo—C_2 bond.

Owing to the formation of the C_1—O_a bond, the negative charge on the O_a atom increases from −0.42 a.u. in **a1** to −0.58 a.u. in **a3**. The C_1 atom is negative (−0.43 a.u.) in the isolated ethene molecule but positive (0.13 a.u.) in the intermediate **a3**, which is due to the formation of a direct bond with the O_a atom of larger electronegativity. An electronic charge of ca. 0.35 a.u. is transferred from the C_2H_4 to the MoO_2 fragments. Accordingly, the formation of the **a3** intermediate can be regarded as the electrophilic attack of the $Mo^{VI}O_2^{2+}$ fragment to the π-bond of the ethene molecule. According to the population analysis, the stages of **a1** → **a2** → **a3** witness the gradual transfer of negative charges from the ethene to the $Mo^{VI}O_2^{2+}$ fragments, consistent with the geometric analysis as described above.

The opening of the four-membered ring in the **a3** intermediate leads to the final product of the Mo-methylidene species (**a5**) and formaldehyde (Scheme 1a). The transition-state structure of the **a3** → **a5** conversion step is denoted as **a4**. It was found that **a4** has a very flat ring with the Mo–C_2–O_a–C_1 dihedral of 178.4°. However, the angle between the oxo-O_b and lattice-O_{11}' ligands, i.e., O_b–Mo–O_{11}', is equal to 144.6° and deviates severely from 180.0° in an ideal TBP geometry, which may be caused by the loosely bound formaldehyde fragment. The comparisons between the bond lengths in structures **a3** and **a4** show that the C_1—C_2 bond is elongated by 0.515 Å and is more obvious than the Mo—O_a bond elongated by 0.094 Å. The Mo center in the Mo-methylidene structure **a5** has one oxo-O_b-ligand, one carbene group and four direct bonds with the lattice-O_z atoms. In **a5**, the Mo–C_2 distance is equal to 1.934 Å, close to the Mo–C lengths of the Mo-methylidene species on the silica and alumina clusters [67,68]. There is little spectroscopic evidence for the metal-carbene species anchored on the surfaces of heterogeneous catalysts. In this work, the C–H-stretching frequencies in **a5** are calculated at 3233.6 and 3125.2 cm^{-1}, well consistent with the reported data of 3225 and 3096 cm^{-1} for the alkylidene moiety on molybdena–alumina [69].

The energy diagram of the whole process; i.e., from the addition of ethene towards the Mo-dioxo active site **a1** to the final product of the Mo-methylidene species **a5**, is graphically presented in Fig. 3. According to the B3LYP/B2//B3LYP/B1 results, the formation of the oxametallacyclobutane **a3** from **a1** is an endothermic process (ΔE = 8.2 kcal mol^{-1}) with a moderate activation barrier (24.4 kcal mol^{-1}). Step 2 occurs with a higher energy barrier (about 34.0 kcal mol^{-1}), since the formation of the product **a5** requires the ruptures of two direct bonds in the oxametallacyclobutane intermediate **a3** (C_1–C_2 = 1.513 Å and Mo–O_a = 1.936 Å). This activation barrier is close to that of the cleavage of the Re-metallaoxetane complex to the Re-carbene species [26,27].

The free energy profile at 400 K is shown in Fig. 4, based on the B3LYP/B1 level of theory and corrected with zero point energies. As expected from the loss of the translational entropy (S) in the bimolecular reaction **a1** + C_2H_4 → **a3**, the Gibbs free energies (G) produces a higher barrier as well as less stable intermediate **a3** and transition state **a2** than predicted from the electronic energies in Fig. 3. The free energy ΔG for Step 1 is estimated at 23.1 kcal mol^{-1},

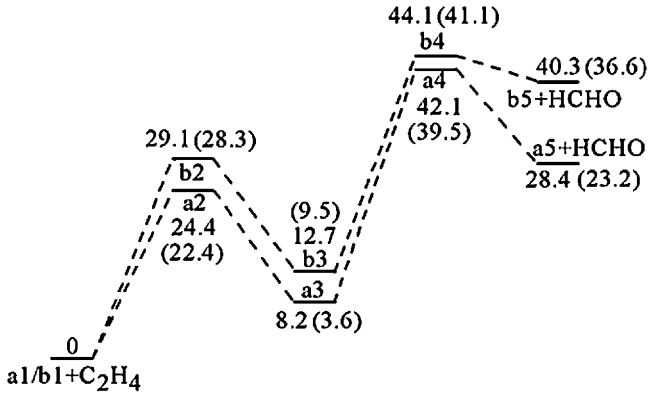

Fig. 3. The potential energy surfaces for the Mo-methylidene formation reaction starting from the Mo(VI) and Mo(V) active sites (energy units in kcal mol^{-1}). The energies of **a1** + C_2H_4 or **b1** + C_2H_4 were set as benchmarks. The relative energies are obtained according to the B3LYP/B2//B3LYP/B1 and B3LYP/B1 (in parentheses) calculations.

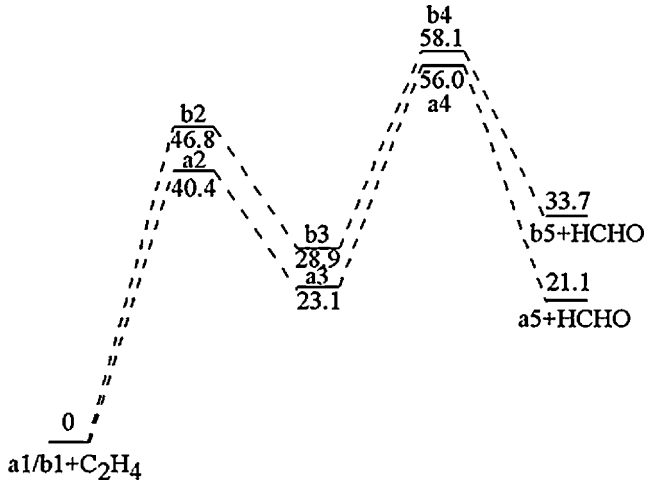

Fig. 4. Comparison of the Gibbs free energies for Mo-methylidene formation reaction starting from the Mo(VI) and Mo(V) active sites (energy units in kcal mol^{-1}). The energies of **a1** + C_2H_4 or **b1** + C_2H_4 were set as benchmarks. The relative energies are obtained according to the B3LYP/B1 calculations.

crossing over a free energy barrier of 40.4 kcal mol^{-1}. Accordingly, the formation of the oxametallacyclobutane intermediate is thermodynamically disfavoured. However, the situation is opposite in Step 2, **a3** → **a5** + HCHO, where the gain in the entropy for a dissociation reaction leads to a lower energy barrier and more stable products **a5** and transition state **a4** than those predicted from the electronic energies in Fig. 3. The decomposition of the TBP intermediate **a3** into the products is slightly exothermic (−2.0 kcal mol^{-1}), overcoming a barrier height of 32.9 kcal mol^{-1}, indicating that the generation of the Mo-carbene species is an energetically advantageous process. It is revealed that the Mo-alkylidene species can be created by ethene and do not require olefins with allylic C—H bonds, which thus provides the direct evidence for the pseudo-Wittig mechanisms in the heterogeneous systems. However, the energy barriers of the present work are relatively high, which can be caused by the low reactivity of ethene. A significant reduction in the energy barriers of Step 2 was observed when 2-butene instead of ethene reacts over the Mo active sites [70].

Table 2
Geometric parameters and Mulliken charges for the energy minima and transition states along the Mo(V)-methylidene formation pathway[a].

	b1	b2	b3	b4	b5
Mo–O_b	1.957	1.898	1.894	1.896	1.880
Mo–O_{11}	2.398	2.272	2.349	2.363	2.381
Mo–O_{11}'	2.209	2.302	2.283	2.427	2.260
Mo–O_{13}	2.140	2.380	2.209	2.313	2.132
Mo–O_{13}'	2.144	2.246	2.207	2.307	2.174
Mo–O_a	1.671	1.771	1.908	2.013	
C_1–C_2		1.421	1.515	2.076	
Mo–C_2		2.273	2.182	1.974	1.908
O_a–C_1		1.894	1.439	1.330	
O_{11}–H	2.202	2.461	2.270	2.703	2.338
O_b–Mo–O_{11}'	177.4	154.2	164.6	145.6	171.5
Mo–C_2–O_a–C_1		−169.6	−168.6	−176.4	
Σα[b]		354.5	354.7	355.2	
q(Mo)	1.43	1.24	1.31	1.21	1.19
q(O_a)	−0.39	−0.54	−0.57	−0.46	
q(O_b)	−0.63	−0.63	−0.63	−0.62	−0.62
q(MoOOH)	0.76	0.41	0.47	0.48	
q(C1)	−0.43	−0.018	0.12	0.041	
q(C2)	−0.43	−0.41	−0.47	−0.49	−0.43
q(C_2H_4)	0.00[c]	0.35	0.27	0.28	

[a] Bond distances in Å and angles, dihedrals in degrees.
[b] The sum of the three angles O_{11}–Mo–O_a, O_a–Mo–C_2 and C_2–Mo–O_{11}.
[c] The data for the isolated ethene molecule.

3.3. Geometric structure of the Mo^V active site

At elevated temperatures, the transformations from the Mo(VI) to Mo(V) active sites can occur in the presence of olefins or other reducing agents. The Mo(V) peak was also detected in the Mo/Al_2O_3 catalysts when the sample was pretreated with an inert gas or alkene [31,32]. The optimized $Mo^VO(OH)$/T1T1 model, **b1**, is shown in Fig. 5 and the selected geometrical parameters are given in Table 2. The terminal Mo=O_a bond is 1.671 Å, slightly shorter than that in the $Mo^{VI}O_2$ monomer. The Mo—OH single bond length is 1.957 Å, close to that reported for the adsorption of H atoms on the oxo groups of Mo_3O_9 clusters [71]. Furthermore, the hydroxyl group is oriented towards the framework O_{11} atom, forming the hydrogen bond with the distance of 2.202 Å.

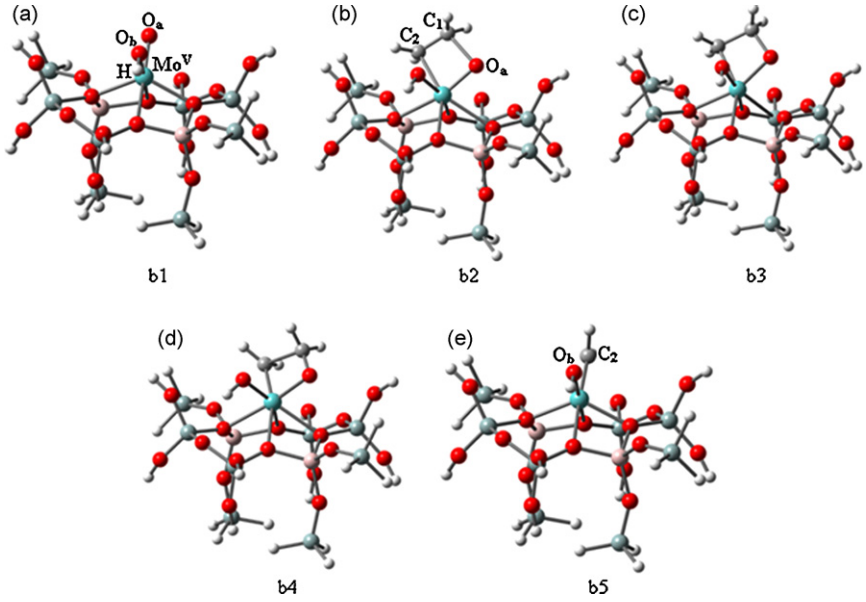

Fig. 5. Energy minima (**b1**, **b3**, **b5**) and transition states (**b2**, **b4**) along the Mo(V)-methylidene formation pathway.

3.4. Mo-methylidene formation over the Mo(V) active site

The geometries of the energy minima and transition states along the reaction pathway are depicted in Fig. 5, and the selected geometrical parameters are given in Table 2. As shown in Scheme 1, the reaction pathway of the Mo(V)-carbene formation on the **b1** active site is analogous to the Mo(VI)-carbene formation on the **a1** active site. The addition of ethene to **b1** produces the oxametallacyclobutane intermediate **b3**, and the following is the cycloreversion resulting in the products of the Mo(V)-methylidene species **b5** and formaldehyde. The comparisons of the energy minima and the transition-state geometries (Figs. 2 and 5) indicate that the reaction pathways on the **a1** and **b1** active sites have many similar characteristics. From the transition structure **b2** to the oxametallacyclobutane intermediate **b3**, the formation of the Mo—C_2 bond is anterior to the C_1—O_a bond, and from **b3** to **b4**, the Mo—O_a bond is less elongated than the C_1—C_2 bond, which are in good agreement with the results of the a series (**a1**–**a5**). The C–H stretching vibrations in **b5** are computed at 3187.6 cm^{-1} and 3076.9 cm^{-1}, also close to the reported values. The structural differences of the b series (**b1**–**b5**) with the **a** series (**a1**–**a5**) are the substitutions of an oxo-O atom with a hydroxyl group, which allows weak interactions with the adjacent lattice-O atoms. In the energy minima **b3** and **b5**, the hydroxyl H atoms form hydrogen bonds with the nearest equatorial lattice-O_{11} atoms with their distances optimized at 2.270 Å and 2.338 Å, respectively. However, the apical O ligands are much more tilted in the transition states **b2** and **b4** ($\angle O_b$–Mo–O_{11}' = 154.2° in **b2** and 145.6° in **b4**, respectively) compared with those in the energy minima **b1** and **b5**, where the $\angle O_b$–Mo–O_{11}' angles are equal to 177.4° and 171.5°, respectively. As a result, the hydroxyl H atoms in the transition states shift away from the lattice-O_{11} atoms and point towards the lattice-O_{32} atoms not belonging to the TBP geometries (Fig. 5). The O_bH—O_{32} hydrogen bonds are calculated at 2.355 in **b2** and 2.141 Å in **b4**, respectively.

Despite the numerous geometrical similarities of the Mo(VI) and Mo(V) pathways, their energy profiles are different as shown in Figs. 3 and 4. With the entry points (**a1** + C_2H_4 and **b1** + C_2H_4) of each pathway set as the benchmark, the other energy minima are more stable in the case of Mo(VI) active site than in the case of Mo(V) active site. That is, the oxametallacyclobutane intermediate **b3** is formed more endothermically (ΔE = 12.7 kcal mol^{-1}, ΔG = 28.9 kcal mol^{-1}) than the corresponding intermediate **a3**. The activation barrier of Step 1 in the Mo(V) active site is also 4.7 kcal mol^{-1} higher in energy than in the Mo(VI) active site. For Step 1, the negative charges transferred are calculated to be 0.35 and 0.29 a.u. for the Mo(VI) and Mo(V) active sites, respectively. As this step is an electrophilic attack, the less transferred charges in the Mo(V) active site will be expected to have higher barriers, which were confirmed by the calculated data discussed earlier. However, the situation is changed for Step 2. At this step, the formation of the Mo(V)-methylidene species has an activation barrier about 2.5 kcal mol^{-1} lower than that of the Mo(VI)-methylidene species, which can be attributed to the less stable intermediate **b3** (Figs. 3 and 4).

3.5. Electronic effects and frontier orbital analysis

As discussed above, the formations of the Mo-methylidene species over the Mo(VI)-dioxo and Mo(V)-monooxo active sites proceed via two independent pathways. The energy barriers of the elementary reaction steps are sensitive to the oxidation states of the Mo centers. The oxo-O_b-ligands present in the a series act as an electron-withdrawing group, which causes the Mo(VI) center more electrophilic and thus conduces to the reduction of energy barriers for the formation of the oxametallacyclobutane intermediate **a3**. Compared with the respective entry points (**a1** + C_2H_4 and **b1** + C_2H_4), the oxametallacyclobutane intermediates are of higher stabilities in the case of the Mo(VI) active site, which however accounts for the higher energy barrier in the following [2 + 2] cycloreversions. The introduction of the hydroxyl group at the Mo(V) active site decreases the positive charge of the Mo(V) center to 1.43 a.u. instead of 1.52 a.u. of the Mo(VI) center, which in turn causes a decreased affinity for the ethene molecule. Meanwhile, the less electropositive Mo(V) center weakens the Mo—O_a bond, so the oxametallacyclobutane intermediate of **b3** is destabilized and results in a lower activation barrier for the subsequent [2 + 2] cycloreversion step.

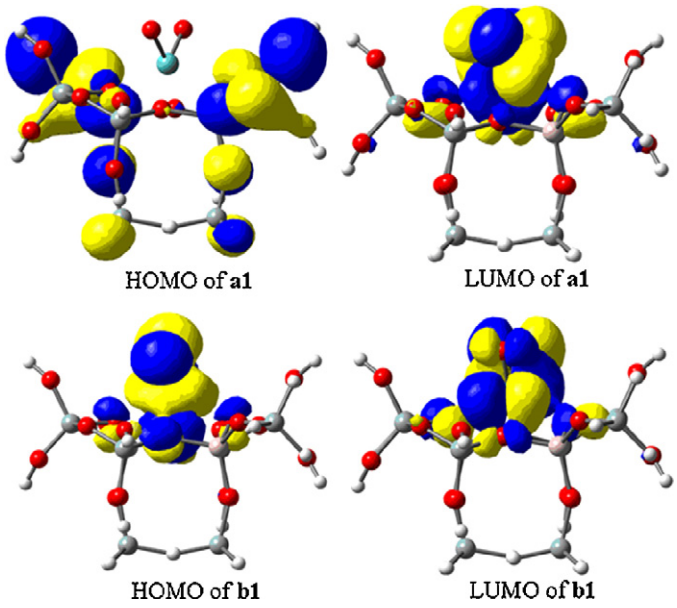

Fig. 6. Isosurfaces of the HOMO (left) and LUMO (right) of the Mo-oxo centers embedded in Beta zeolite.

In both reaction pathways, the activation barriers of Step 2 are estimated to be higher than those of Step 1 (Fig. 3). The overall free energy barriers at B3LYP/B1 level are calculated at 56.0 and 58.1 kcal mol^{-1} on the Mo(VI) and Mo(V) active sites, respectively (Fig. 4). That is, the activation barrier is slightly lower in the case of the Mo(VI) active site. In addition, their reaction heats for the overall process are estimated to be 21.1 and 33.7 kcal mol^{-1}, respectively, which indicates that the process on the Mo(VI) active site is much preferred in thermodynamics. Accordingly, the Mo(VI) active site rather than the Mo(V) active site is more efficient in catalyzing the formation of the Mo-carbene species, and therefore the Mo-methylidene species is more likely to form with the Mo center of +VI oxidation state.

The isosurfaces of the frontal molecular orbitals of the two Mo-oxo centers are presented in Fig. 6. The highest occupied molecular orbital (HOMO) of **a1** is related to the p orbitals of the lattice-O atoms, whereas the lowest unoccupied molecular orbital (LUMO) is predominantly from the Mo d-orbitals. In **b1**, the shape and size of the HOMO and LUMO differ significantly from those of **a1**. The HOMO is composed of the d_{xy} orbital of the Mo(V) center and the p_y orbital of the oxo-O_b atom, while the LUMO is attributed to the d_{z^2} orbital of the Mo(V) center. Obviously, the HOMO of **a1** is not involved in the reaction process, and therefore it is very likely for **a1** to offer LUMO to interact with the HOMO of the incoming ethene molecule. It is consistent with the above Mulliken charge analysis and supports the electrophilic nature. In addition, the energy gap between the HOMO of ethene and the LUMO of **a1** is calculated at 0.13 a.u. and 0.02 a.u. lower than that to **b1**, which indicates

the slightly higher reactivity of **a1** than **b1** towards the ethene molecule.

4. Conclusions

The reaction mechanisms of the Mo-methylidene formation over the Mo/HBeta zeolite catalysts were studied with density functional methods. Two different Mo active sites, the oxidized form $Mo^{VI}O_2$ and the reduced form $Mo^{V}O(OH)$, were considered. It was found that the Mo-carbene formations are divided into two elementary reaction steps via the pseudo-Wittig mechanism: Step 1 is the endothermic formation of the oxametallacyclobutane intermediates through the [2 + 2] cycloaddition between the C=C bonds in ethene and Mo=O_a bonds in the Mo active sites; Step 2 is the opening of the four-membered rings in the oxametallacyclobutane intermediates producing the Mo-methylidene species. The activation barriers of Step 2 were estimated to be higher than Step 1: 33.9 kcal mol^{-1} vs. 24.4 kcal mol^{-1} and 31.4 kcal mol^{-1} vs. 29.1 kcal mol^{-1} on the Mo(VI) and Mo(V) active sites, respectively. In addition, it was revealed that Mo-alkylidene species can be created by ethene and do not require olefins with allylic C—H bonds, which substantiates the pseudo-Wittig mechanisms in heterogeneous systems.

The reactivities of the Mo active sites were dependent on their oxidation states, which were elucidated by the electronic properties of the O_b-ligands bonded to the Mo centers. Step 1 was facilitated by the electron-withdrawing O_b-ligand in the Mo(VI) active site; instead, Step 2 was more facile in the Mo(V) active site owing to the destabilized Mo-oxametallacyclobutane intermediates caused by the presence of the electron-donating –O_bH group. For the whole processes of generating the Mo-methylidene species from the Mo active sites, both of the free energy barriers and reaction heats were found to be lower in the Mo(VI) rather than in the Mo(V) active site, indicating that the initiation reaction over the Mo(VI) active site was preferred. Accordingly, the Mo(VI) active site was more efficient in producing the Mo(VI)-methylidene species over the Mo/HBeta catalysts.

Acknowledgments

We gratefully acknowledge the financial support of the National Natural Science Foundation of China (grants 20403017 and 20303019) and the Ministry of Science and Technology of China through the National Key Project of Fundamental Research (Grant 2003CB615806). The authors thank Jason White from UCSB for helpful discussions.

References

[1] Y.Y. Shu, D. Ma, L.Y. Xu, Y.D. Xu, X.H. Bao, Catal. Lett. 70 (2000) 67.
[2] F. Solymosi, A. Erdohelyi, A. Szoke, Catal. Lett. 32 (1995) 43.
[3] P. Kovacheva, N. Davidova, J. Novakova, Zeolites 11 (1991) 54.
[4] S.L. Liu, S.J. Huang, W.J. Xin, J. Bai, S.J. Xie, L.Y. Xu, Catal. Today 93–95 (2004) 471.
[5] J.L. Lemberton, N. Gnofam, G. Perot, Appl. Catal. A 90 (1992) 175.
[6] X.J. Li, W.P. Zhang, S.L. Liu, X.W. Han, L.Y. Xu, X.H. Bao, J. Mol. Catal. A: Chem. 250 (2006) 94.
[7] X.J. Li, W.P. Zhang, S.L. Liu, L.Y. Xu, X.W. Han, X.H. Bao, J. Catal. 250 (2007) 55.
[8] B.N. Shelimov, I.V. Elev, V.B. Kazansky, J. Mol. Catal. 46 (1988) 187.
[9] K.A. Vikulov, B.N. Shelimov, V.B. Kazansky, J. Mol. Catal. 65 (1991) 393.
[10] K.A. Vikulov, B.N. Shelimov, V.B. Kazansky, J.C. Mol, J. Mol. Catal. 90 (1994) 61.
[11] A.K. Rappé, W.A. Goddard III, J. Am. Chem. Soc. 104 (1982) 448.
[12] Y. Iwasawa, H. Kubo, H. Hamamura, J. Mol. Catal. 28 (1985) 191.
[13] J. Engelhardt, J. Goldwasser, W.K. Hall, J. Catal. 70 (1985) 364.
[14] R.H. Grubbs, S.J. Swetnick, J. Mol. Catal. 8 (1980) 25.
[15] E.A. Lombardo, M. Houalla, W.K. Hall, J. Catal. 51 (1978) 256.
[16] A.K. Rappé, W.A. Goddard III, J. Am. Chem. Soc. 102 (1980) 5114.
[17] J.R. McCoy, M.F. Farona, J. Mol. Catal. 66 (1991) 51.
[18] D.T. Laverty, J.J. Rooney, A. Stewart, J. Catal. 45 (1976) 110.
[19] X.Y. Chen, X.Y. Zhang, P. Chen, Angew. Chem. Int. Ed. 42 (2003) 3798.
[20] J. Handzlik, J. Ogonowski, Catal. Lett. 88 (2003) 119.
[21] A. Brenner, R.L.J. Burwell, J. Catal. 52 (1978) 364.
[22] A. Salameh, C. Coperet, J.M. Basset, V.P.W. Bohm, M. Roper, Adv. Synth. Catal. 349 (2007) 238.
[23] D.V. Deubel, G. Frenking, J. Am. Chem. Soc. 121 (1999) 2021.
[24] M.A. Pietsch, T.V. Russo, R.B. Murphy, R.L. Martin, A.K. Rappé, Organometallics 17 (1998) 2716.
[25] X. Zhang, X. Chen, P. Chen, Organometallics 23 (2004) 3437.
[26] X. Zhang, S. Narancic, P. Chen, Organometallics 24 (2005) 3040.
[27] S. Narancic, P. Chen, Organometallics 24 (2005) 10.
[28] K.P. Gable, T.N. Phan, J. Am. Chem. Soc. 116 (1994) 833.
[29] A.K. Rappé, W.A. Goddard III, Nature 285 (1980) 311.
[30] W. Grüenert, R. Feldhaus, K. Anders, E.S. Shpiro, K.M. Minachev, J. Catal. 120 (1989) 444.
[31] W. Grüenert, A.Y. Stakheev, R. Feldhaus, K. Anders, E.S. Shpiro, K.M. Minachev, J. Catal. 135 (1992) 287.
[32] B.A. Zhang, Y.S. Li, Q.S. Lin, D. Jin, J. Mol. Catal. 46 (1988) 229.
[33] Y. Iwasawa, H. Ichinose, S. Ogasawara, M. Soma, J. Chem. Soc., Faraday Trans. 177 (1981) 1763.
[34] Y. Iwasawa, S. Ogasawara, J. Chem. Soc., Faraday Trans. 175 (1979) 1465.
[35] K.A. Vikulov, I.V. Elev, B.N. Shelimov, V.B. Kazansky, J. Mol. Catal. 55 (1989) 126.
[36] K.A. Vikulov, I.V. Elev, B.N. Shelimov, V.B. Kazansky, Catal. Lett. 2 (1989) 121.
[37] J.M. Newsam, M.M.J. Treacy, W.T. Koetsier, C.B. De Gruyter, Proc. R. Soc. London, A 420 (1988) 375.
[38] J.B. Higgins, R.B. Lapierre, J.L. Schlenker, A.C. Rohrman, J.D. Wood, G.T. Kerr, W.J. Rohrbaugh, Zeolites 8 (1988) 446.
[39] J. Dedecek, L. Capek, D. Kaucky, Z. Sobalık, B. Wichterlova, J. Catal. 211 (2002) 198.
[40] J. Penzien, A. Abraham, J.A. van Bokhoven, A. Jentys, T.E. Muller, C. Sievers, J.A. Lercher, J. Phys. Chem. B 108 (2004) 4116–4126.
[41] J.A. van Bokhoven, D.C. Koningsberger, P. Kunkeler, H. van Bekkum, A.P.M. Kentgens, J. Am. Chem. Soc. 122 (2000) 12842.
[42] D. Berthomieu, S. Krishnamurty, B. Coq, G. Delahay, A. Goursot, J. Phys. Chem. B 105 (2001) 1149.
[43] A. Martinez, A. Goursot, B. Coq, G. Delahay, J. Phys. Chem. B 108 (2004) 8823.
[44] A. Goursot, B. Coq, F. Fajula, J. Catal. 216 (2003) 324.
[45] A.L. Yakovlev, G.M. Zhidomirov, R.A. van Santen, J. Phys. Chem. B 105 (2001) 12297.
[46] L. Rodriguez-Santiago, M. Sierka, V. Branchadell, M. Sodupe, J. Sauer, J. Am. Chem. Soc. 120 (1998) 1545.
[47] P. Pietrzyk, Z. Sojka, S. Dzwigaj, M. Che, J. Am. Chem. Soc. 129 (2007) 14174.
[48] A.D. Becke, Phys. Rev. A 38 (1988) 3098.
[49] A.D. Becke, J. Chem. Phys. 98 (1993) 5648.
[50] B. Miehlich, A. Savin, H. Stoll, H. Preuss, Chem. Phys. Lett. 157 (1989) 200.
[51] C. Lee, W. Yang, G. Parr, Phys. Rev. B 37 (1988) 785.
[52] P.J. Hay, W.R. Wadt, J. Chem. Phys. 82 (1985) 299.
[53] K. Wada, C.B. Pamplin, P. Legzdins, B.O. Patrick, I. Tsyba, R. Bau, J. Am. Chem. Soc. 125 (2003) 7035.
[54] A.W. Ehlers, M. Biihme, S. Dapprich, A. Gobbi, A. Hijllwarth, V. Jonas, K.F. Kiihler, R. Stegmann, A. Veldkamp, G. Frenking, Chem. Phys. Lett. 208 (1993) 111.
[55] D.V. Deubel, J. Sundermeyer, G. Frenking, J. Am. Chem. Soc. 122 (2000) 10101.
[56] M.J. Frisch, G.W. Trucks, H.B. Schlegel, G.E. Scuseria, M.A. Robb, J.R. Cheeseman, V.G. Zakrzewski, J.A. Montgomery, R.E. Stratmann, J.C. Burant, S. Dapprich, J.M. Millam, A.D. Daniels, K.N. Kudin, M.C. Strain, O. Farkas, J. Tomasi, V. Barone, M. Cossi, R. Cammi, B. Mennucci, C. Pomelli, C. Adamo, S. Clifford, J. Ochterski, G.A. Petersson, P.Y. Ayala, Q. Cui, K. Morokuma, D.K. Malick, A.D. Rabuck, K. Raghavachari, J.B. Foresman, J. Cioslowski, J.V. Ortiz, B.B. Stefanov, G. Liu, A. Liashenko, P. Piskorz, I. Komaromi, R. Gomperts, R.L. Martin, D.J. Fox, T. Keith, M.A. Al-Laham, C.Y. Peng, A. Nanayakkara, C. Gonzalez, M. Challacombe, P.M.W. Gill, B.G. Johnson, W. Chen, M.W. Wong, J.L. Andres, M. Head-Gordon, E.S. Replogle, J.A. Pople, Gaussian98 (Revision A.9), Gaussian, Inc., Pittsburgh, PA, 1998.
[57] M.M. Huang, R.F. Howe, J. Catal. 108 (1987) 283.
[58] R.W. Borry III, Y.H. Kim, A. Huffsmith, J.A. Reimer, E. Iglesia, J. Phys. Chem. B 103 (1999) 5787.
[59] D. Ma, Q.J. Zhu, Z. Wu, D.H. Zhou, Y.Y. Shu, Q. Xin, Y.D. Xu, X.H. Bao, Phys. Chem. Chem. Phys. 7 (2005) 3102.
[60] D. Berthomieu, J.-M. Ducere, A. Goursot, J. Phys. Chem. B 106 (2002) 7483.
[61] A.L. Yakovlev, A.A. Shubin, G.M. Zhidomirov, R.A. van Santen, Catal. Lett. 70 (2000) 175.
[62] L. Benco, T. Bucko, R. Grybos, J. Hafner, Z. Sobalik, J. Dedecek, J. Hrusak, J. Phys. Chem. C 111 (2007) 586.
[63] L. Benco, T. Bucko, R. Grybos, J. Hafner, Z. Sobalik, J. Dedecek, S. Sklenak, J. Hrusak, J. Phys. Chem. C 111 (2007) 9393.
[64] G. Fischer, A. Goursot, B. Coq, G. Delahay, S. Pal, Chem. Phys. Chem. 7 (2006) 1795.
[65] W. Li, G.D. Meitzner, R.W. Borry III, E. Iglesia, J. Catal. 191 (2000) 373.
[66] T. Sasaki, F. Nakagawa, Y. Iwasawa, J. Phys. Chem. B 109 (2005) 2128.
[67] J. Handzlik, J. Ogonowski, R. Tokarz-Sobieraj, Catal. Today 101 (2005) 163.
[68] J. Handzlik, J. Phys. Chem. B 109 (2005) 20794.
[69] J. Handzlik, J. Catal. 220 (2003) 23.
[70] J. Guan, G. Yang, D.H. Zhou, W.P. Zhang, X.C. Liu, X.W. Han, X.H. Bao, Catal. Comm. 9 (2008) 2213.
[71] Y.H. Jang, W.A. Goddard, J. Phys. Chem. B 106 (2002) 5997.